The Plant Membrane-Associated REMORIN1.3 Accumulates in Discrete Perihaustorial Domains and Enhances Susceptibility to *Phytophthora infestans*[1][W]

Tolga O. Bozkurt, Annis Richardson, Yasin F. Dagdas, Sébastien Mongrand, Sophien Kamoun, and Sylvain Raffaele*

Sainsbury Laboratory, Norwich NR4 7UH, United Kingdom (T.O.B., A.R., Y.F.D., S.K., S.R.); Department of Life Sciences, Imperial College London, London SW7 2AZ, United Kingdom (T.O.B.); John Innes Centre, Norwich NR4 7UH, United Kingdom (A.R.); Laboratoire de Biogenèse Membranaire, Unité Mixte de Recherche 5200 Centre National de la Recherche Scientifique-Université Bordeaux Segalen-Institut National de la Recherche Agronomique, F–33883 Villenave d'Ornon cedex, France (S.M.); and Laboratoire des Interactions Plantes-Microorganismes, Unité Mixte de Recherche 441 Institut National de la Recherche Agronomique-Unité Mixte de Recherche 2594 Centre National de la Recherche Scientifique, F–31326 Castanet-Tolosan, France (S.R.)

Filamentous pathogens such as the oomycete *Phytophthora infestans* infect plants by developing specialized structures termed haustoria inside the host cells. Haustoria are thought to enable the secretion of effector proteins into the plant cells. Haustorium biogenesis, therefore, is critical for pathogen accommodation in the host tissue. Haustoria are enveloped by a specialized host-derived membrane, the extrahaustorial membrane (EHM), which is distinct from the plant plasma membrane. The mechanisms underlying the biogenesis of the EHM are unknown. Remarkably, several plasma membrane-localized proteins are excluded from the EHM, but the remorin REM1.3 accumulates around *P. infestans* haustoria. Here, we used overexpression, colocalization with reporter proteins, and superresolution microscopy in cells infected by *P. infestans* to reveal discrete EHM domains labeled by REM1.3 and the *P. infestans* effector AVRblb2. Moreover, SYNAPTOTAGMIN1, another previously identified perihaustorial protein, localized to subdomains that are mainly not labeled by REM1.3 and AVRblb2. Functional characterization of REM1.3 revealed that it is a susceptibility factor that promotes infection by *P. infestans*. This activity, and REM1.3 recruitment to the EHM, require the REM1.3 membrane-binding domain. Our results implicate REM1.3 membrane microdomains in plant susceptibility to an oomycete pathogen.

Filamentous plant pathogens, including oomycetes of the genus *Phytophthora*, downy mildews and white rusts, as well as powdery mildews and rust fungi, are among the most devastating plant pathogens. These biotrophic parasites associate closely with plant cells through specialized infection structures called haustoria. Haustoria are specialized pathogen hyphal structures formed within host cells and enveloped by a perimicrobial membrane called the extrahaustorial membrane (EHM), a key interface between plant pathogens and the host cell. Haustoria are critical for successful parasitic infection by many filamentous plant pathogens and are a signature of the biotrophic lifestyle. In fungi, haustoria function as feeding structures (Voegele et al., 2001). In addition, haustoria are thought to enable the delivery of host-translocated virulence proteins, known as effectors, by both fungal and oomycete pathogens (Catanzariti et al., 2006; Whisson et al., 2007). However, little is known about the molecular mechanisms underlying the biogenesis and function of haustoria and EHM (Kemen and Jones, 2012; Lu et al., 2012).

The EHM is thought to be continuous with the host plasma membrane (PM), yet it is a highly specialized membrane compartment that develops only in plant cells that accommodate haustoria (haustoriated cells; Coffey and Wilson, 1983). On the plant side, all eight PM proteins tested by Koh et al. (2005) were excluded from the EHM in Arabidopsis (*Arabidopsis thaliana*) cells infected with the powdery mildew fungus *Golovinomyces cichoracearum*. Conversely, the atypical Arabidopsis resistance protein Resistance to Powdery Mildew8.2 (RPW8.2) exclusively localizes to the EHM in this interaction (Wang et al., 2009). Ultrastructure analyses of the *Golovinomyces orontii* powdery mildew pathosystem revealed that the EHM is asymmetric, thicker and more electron opaque than the PM, and can be highly convoluted around mature haustoria (Micali et al., 2011). More recently, a survey of Arabidopsis and

[1] This work was supported by the Gatsby Charitable Foundation, the European Research Council, the Biotechnology and Biological Sciences Research Council, and by Marie Curie Intra European Fellowships (contract no. 268419 to T.O.B. and contract no. 255104 to S.R.).

* Address correspondence to sylvain.raffaele@toulouse.inra.fr.

The author responsible for distribution of materials integral to the findings presented in this article in accordance with the policy described in the Instructions for Authors (www.plantphysiol.org) is: Sylvain Raffaele (sylvain.raffaele@toulouse.inra.fr).

[W] The online version of this article contains Web-only data.
www.plantphysiol.org/cgi/doi/10.1104/pp.114.235804

Nicotiana benthamiana plants infected by the oomycete pathogens *Hyaloperonospora arabidopsidis* and *Phytophthora infestans*, respectively, revealed that several integral host PM proteins are excluded from the EHM (Lu et al., 2012). Nevertheless, the remorin REM1.3 and the SYNAPTOTAGMIN1 (SYT1) peripheral membrane proteins localized to undetermined subcellular compartments around haustoria in *P. infestans*-plant interactions (Lu et al., 2012). Whether the differential accumulation of membrane proteins at the EHM is due to interference with the lateral diffusion of proteins from the PM or targeted secretion of specialized vesicles remains unclear (Lu et al., 2012).

The subcellular distribution of effectors inside plant cells provides valuable clues about the host cell compartments they modify to promote disease, and effectors have emerged as useful molecular probes for plant cell biology (Whisson et al., 2007; Bozkurt et al., 2012). Heterologous expression of fluorescently tagged effectors in plant cells has been used to determine their subcellular localization in uninfected and infected tissue. This approach has been successful with the RXLR and CRINKLER (CRN) effectors, the two major classes of cytoplasmic (host-translocated) oomycete effectors (Bozkurt et al., 2012). The 49 *H. arabidopsidis* RXLR effectors studied by Caillaud et al. (2012) localized to the nucleus, the cytoplasm, or various plant membrane compartments. In contrast, CRN effectors from several oomycete species exclusively accumulate in the plant cell nucleus (Schornack et al., 2010; Stam et al., 2013). The *P. infestans* effectors AVRblb2 and AVR2 accumulate around haustoria when expressed in infected *N. benthamiana* cells, highlighting the PM and the EHM as important sites for effector activity (Bozkurt et al., 2011; Saunders et al., 2012). These effectors, therefore, can serve as useful probes for plant cell biology to dissect vesicular trafficking and focal immunity, processes that have proved difficult to study using standard genetic approaches (Bozkurt et al., 2011; Win et al., 2012).

REM1.3 is one of two plant membrane-associated proteins detected around haustoria during the interaction between *P. infestans* and the model plant *N. benthamiana* (Lu et al., 2012). Therefore, we hypothesized that studying REM1.3 should prove useful for understanding the mechanisms governing the function and formation of perihaustorial membranes. REM1.3 belongs to a diverse family of plant-specific proteins containing a Remorin_C domain (PF03763) and has known orthologs in potato (*Solanum tuberosum*; StREM1.3), tomato (*Solanum lycopersicum*; SlREM1.2), tobacco (*Nicotiana tabacum*; NtREM1.2), and Arabidopsis (AtREM1.1–AtREM1.4; Raffaele et al., 2007). Several proteins from the remorin family, including REM1.3, are preferentially associated with membrane rafts, nanometric sterol- and sphingolipid-rich domains in PMs (Pike, 2006; Simons and Gerl, 2010). Indeed, StREM1.3 and NtREM1.2 are highly enriched in detergent-insoluble membranes (DIMs) and form sterol-dependent domains of approximately 75 nm in purified PMs (Mongrand et al., 2004; Shahollari et al., 2004; Raffaele et al., 2009). StREM1.3 directly binds to the cytoplasmic leaflet of the PM through a C-terminal anchor domain (RemCA) that folds into a hairpin of aliphatic α-helices in polar environments (Raffaele et al., 2009; Perraki et al., 2012). StREM1.3 is differentially phosphorylated upon the perception of polygalacturonic acid (Reymond et al., 1996). AtREM1.3 is differentially recruited to DIMs and differentially phosphorylated upon flg22 (for flagellin) peptide perception (Benschop et al., 2007; Keinath et al., 2010; Marín et al., 2012), suggesting a role in plant defense signaling. StREM1.3 and SlREM1.2 prevent *Potato virus X* spreading by interacting with the Triple Gene Block protein1 (TGBp1) viral movement protein, presumably in plasmodesmata or at the PM (Raffaele et al., 2009; Perraki et al., 2012). AtREM1.2 belongs to protein complexes formed by a negative regulator of immune responses, Resistance to *Pseudomonas syringae* pv *maculicola*1 (RPM1)-INTERACTING PROTEIN4, at the PM (Liu et al., 2009). Furthermore, *Medicago truncatula* MtSYMREM1 is enriched in root cell DIMs (Lefebvre et al., 2007) and localizes to patches at the peribacteroid membrane during symbiosis with *Sinorhizobium meliloti* (Lefebvre et al., 2010). MtSYMREM1 is important for nodule formation and interacts with the Lysin motif domain–containing receptor-like kinase3 (LYK3) symbiotic receptor (Lefebvre et al., 2010). Multiple lines of evidence, therefore, implicate several remorins in cell surface signaling and the accommodation of microbes during plant-microbe interactions (Raffaele et al., 2007; Jarsch and Ott, 2011; Urbanus and Ott, 2012). Nevertheless, little is known about REM1.3's molecular function, and its role in immunity against filamentous plant pathogens has not been reported to date.

In this study, we analyzed in detail the localization and function of REM1.3 during host colonization by *P. infestans*. We found that REM1.3 localizes exclusively to the vicinity of the PM and the EHM around non-callosic haustoria. Furthermore, our results suggest that the EHM is likely formed by multiple microdomains. REM1.3 silencing and overexpression experiments demonstrated that it promotes susceptibility to *P. infestans* in *N. benthamiana* and tomato. We also show that the REM1.3 membrane anchor domain is required for its localization at the EHM and for the promotion of susceptibility to *P. infestans*. This work demonstrates the importance of the dynamic reorganization of the PM in response to haustoria-forming pathogens. Our study also revealed that the effector AVRblb2 localizes to remorin-containing host membrane domains at the host-pathogen interface, possibly as a pathogen strategy to facilitate the accommodation of infection structures inside plant cells.

RESULTS

REM1.3 Localizes at the PM and the EHM in Cells Infected by *P. infestans*

N. benthamiana is a versatile host system in which to study the cellular and molecular dynamics of the plant

response to the hemibiotrophic pathogen *P. infestans* (Chaparro-Garcia et al., 2011; Lu et al., 2012). Using fluorescent markers for the cytoplasm, tonoplast, and EHM, it was found that these three subcellular compartments occur closely around *P. infestans* haustoria (Bozkurt et al., 2012; Caillaud et al., 2012), which makes the distinction between the EHM and these other compartments challenging. To determine in which perihaustorial compartment REM1.3 resides, we performed a series of colocalization studies using various marker proteins labeling distinct perihaustorial compartments in *N. benthamiana* plants inoculated by *P. infestans*. First, to determine the extent to which REM1.3 localizes to the EHM or the cytoplasm surrounding the EHM, we coexpressed red fluorescent protein (RFP):REM1.3 and GFP in infected plant cells by *Agrobacterium tumefaciens*-mediated transient transformation under the control of the cauliflower mosaic virus (CaMV) *35S* promoter. At 4 d post inoculation (dpi), RFP:REM1.3 surrounded *P. infestans* haustoria tightly and showed a sharp and focused signal in contrast to the diffuse cytosolic localization pattern of free GFP, suggesting that REM1.3 localizes specifically at the EHM (Fig. 1A). Second, to exclude the possibility that REM1.3 accumulates at the tonoplast surrounding the EHM, we coexpressed RFP:REM1.3 with the *H. arabidopsidis* effector HaRXL17, which marks the perihaustorial tonoplast in host cells challenged with *P. infestans* (Bozkurt et al., 2012; Caillaud et al., 2012; Fig. 1B). At 4 dpi, RFP:REM1.3 fluorescence was tightly surrounded by GFP:HaRXL17 fluorescence. In plots measuring fluorescence along a line cutting through a haustorium, the two peaks of RFP:REM1.3 fluorescence were located between the two peaks of GFP:HaRXL17, indicating that REM1.3 localizes between the tonoplast and the haustorium. Finally, we coexpressed yellow fluorescent protein (YFP):REM1.3 with the *P. infestans* RXLR effector AVRblb2 that associates with the EHM in infected plant cells (Bozkurt et al., 2011, 2012; Fig. 1C). Remarkably, REM1.3 and AVRblb2 colocalized almost completely around the haustorium, further highlighting the association of REM1.3 with the EHM.

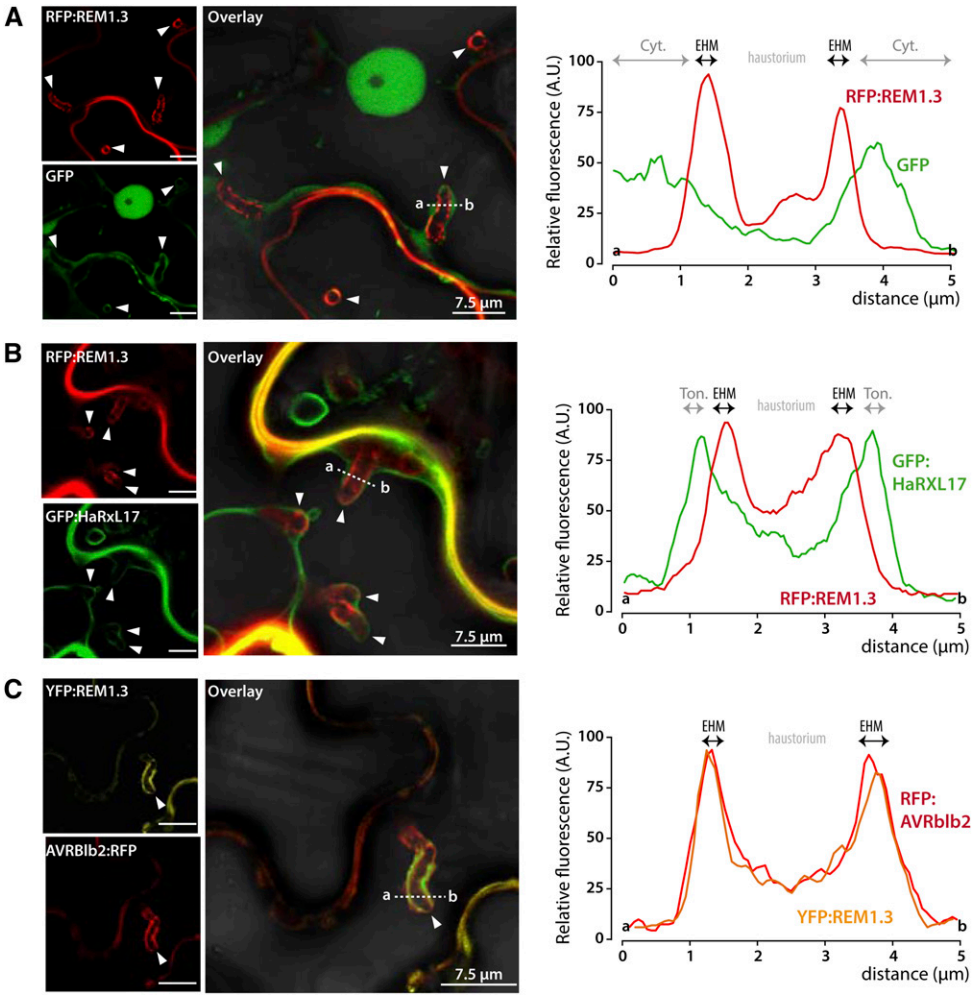

Figure 1. REM1.3 localizes at the PM and the EHM in cells infected by *P. infestans*. Coexpression of RFP:REM1.3 and GFP (A), RFP:REM1.3 and GFP:HaRXL17 (B), and YFP:REM1.3 and RFP:AVRblb2 (C) by *A. tumefaciens*-mediated transient transformation under the control of the CaMV *35S* promoter in haustoriated cells discriminates between host subcellular compartments surrounding haustoria. GFP, HaRXL17, and AVRblb2 label the cytoplasm and nucleus, the tonoplast, and the EHM and PM, respectively. Colocalization is only observed between REM1.3 and AVRblb2. Images show single optical sections. The fluorescence plots show relative fluorescence along the dotted line connecting points a and b. Arrowheads point to the tips of haustoria. A.U., Arbitrary units; Cyt., cytoplasm; Ton., tonoplast. Bars = 7.5 μm.

REM1.3 Accumulates around Noncallosic Haustoria during Infection by *P. infestans*

To document the robustness and dynamics of REM1.3 localization at the EHM, we used *N. benthamiana* transgenic plants constitutively expressing YFP:REM1.3 (Lu et al., 2012). We inoculated these plants with the transgenic *P. infestans* isolate 88069 constitutively expressing RFP (88069td; Chaparro-Garcia et al., 2011) and monitored the distribution of YFP:REM1.3 in infected cells. We observed in approximately 50% (102 out of 197 cases) that haustoria were surrounded by REM1.3, while in the rest of the cases, REM1.3 only remained at the adjacent PM (Fig. 2A). To further analyze REM1.3 localization at the EHM, we compared its perihaustorial distribution with that of AVRblb2. When coexpressed, YFP:REM1.3 was detected at the EHM in nearly 50% of the cases (seven out of 16 observations), while RFP-AVRblb2 always localized at the EHM (16 out of 16; Fig. 2B).

Unlike the haustoria of powdery mildew fungi and *H. arabidopsidis*, *P. infestans* haustoria are rarely surrounded by callose encasements but sometimes accumulate a callosic collar (Bozkurt et al., 2011). Callose encasements are thought to be indicative of a plant defense reaction and do not reflect an active and functional haustorial interface (van Damme et al., 2009). To determine the degree to which REM1.3 perihaustorial accumulation is associated with callose, we performed aniline blue staining on plants expressing YFP:REM1.3 and infected by a *P. infestans* strain (88069td) expressing a cytosolic RFP. REM1.3-labeled haustoria did not display a callosic collar (Fig. 2C), indicating that the perihaustorial localization of REM1.3 is not due to encasement of the haustoria. This suggests that REM1.3 could play a role in the control of the infection process via the suppression of callose deposition or other unknown mechanisms.

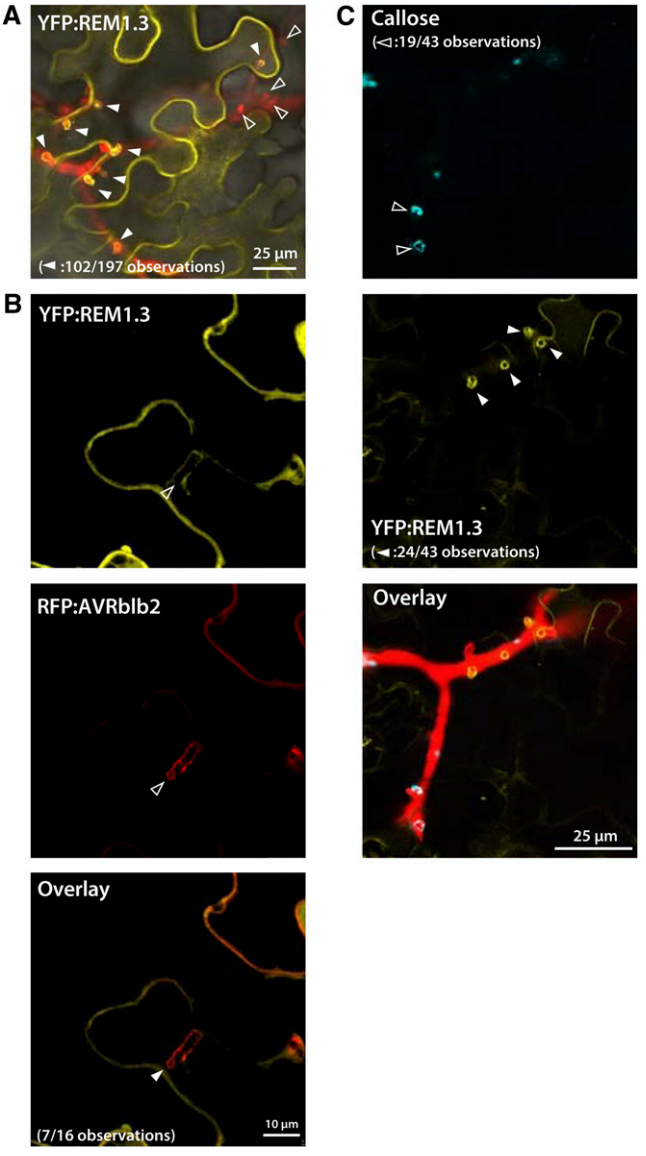

Figure 2. REM1.3 localizes around a subpopulation of noncallosic haustoria during *P. infestans* infection. A, Representative image of a stable *35S*-YFP:REM1.3 *N. benthamiana* transgenic plant inoculated by *P. infestans* strain 88069 expressing RFP (88069td). Haustoria are indicated with closed arrowheads when surrounded by YFP:REM1.3 and with open arrowheads otherwise. B, Frequency of the colocalization of YFP:REM1.3 with RFP:AVRblb2 around *P. infestans* haustoria. YFP:REM1.3 with RFP:AVRblb2 constructs were codelivered into *N. benthamiana* leaves by *A. tumefaciens*-mediated transformation. C, *P. infestans* 88069td-inoculated leaves expressing YFP:REM1.3 and stained for callose. Haustoria surrounded by YFP:REM1.3 (closed arrowheads) never showed a callose neck band (open arrowheads). Images show single optical sections. The frequency of observations is indicated.

REM1.3 Colocalizes with the *P. infestans* RXLR Effector AVRblb2 in Specific Domains at the EHM

REM1.3 is a well-established protein marker of sterol- and sphingolipid-rich PM domains designated as membrane rafts (Raffaele et al., 2009). We observed that REM1.3 displays nonuniform perihaustorial accumulation, delimiting discrete membrane domains at the EHM (Fig. 1). Similar to REM1.3, the *P. infestans* RXLR effector AVRblb2 localizes to the PM and dramatically relocalizes to the EHM during host infection (Bozkurt et al., 2011, 2012). We observed that REM1.3 and AVRblb2 significantly colocalize at the EHM in haustoria cross sections (Fig. 1). To test whether AVRblb2 specifically targets REM1.3-containing membrane domains, we examined the degree to which these two proteins colocalize in haustoria longitudinal sections. For this, we coexpressed YFP:REM1.3 and RFP:AVRblb2 in *N. benthamiana*-infected cells at 4 dpi. Both RFP:AVRblb2 and YFP:REM1.3 distributed heterogenously around haustoria-forming perihaustorial foci. The more intense RFP:AVRblb2 foci colocalized with YFP:REM1.3 foci (Fig. 3A, arrowheads). To quantify the degree of REM1.3 and AVRblb2 colocalization, we extracted fluorescence

signals along the EHM and calculated Pearson correlation coefficients (ρ values; Fig. 3B). The average Pearson correlation coefficient between the YFP and RFP fluorescence signals around haustoria was 0.79, indicating that REM1.3 and AVRblb2 are present at the same perihaustorial domains.

To further define the membrane perihaustorial domains, we coexpressed REM1.3 and AVRblb2 with

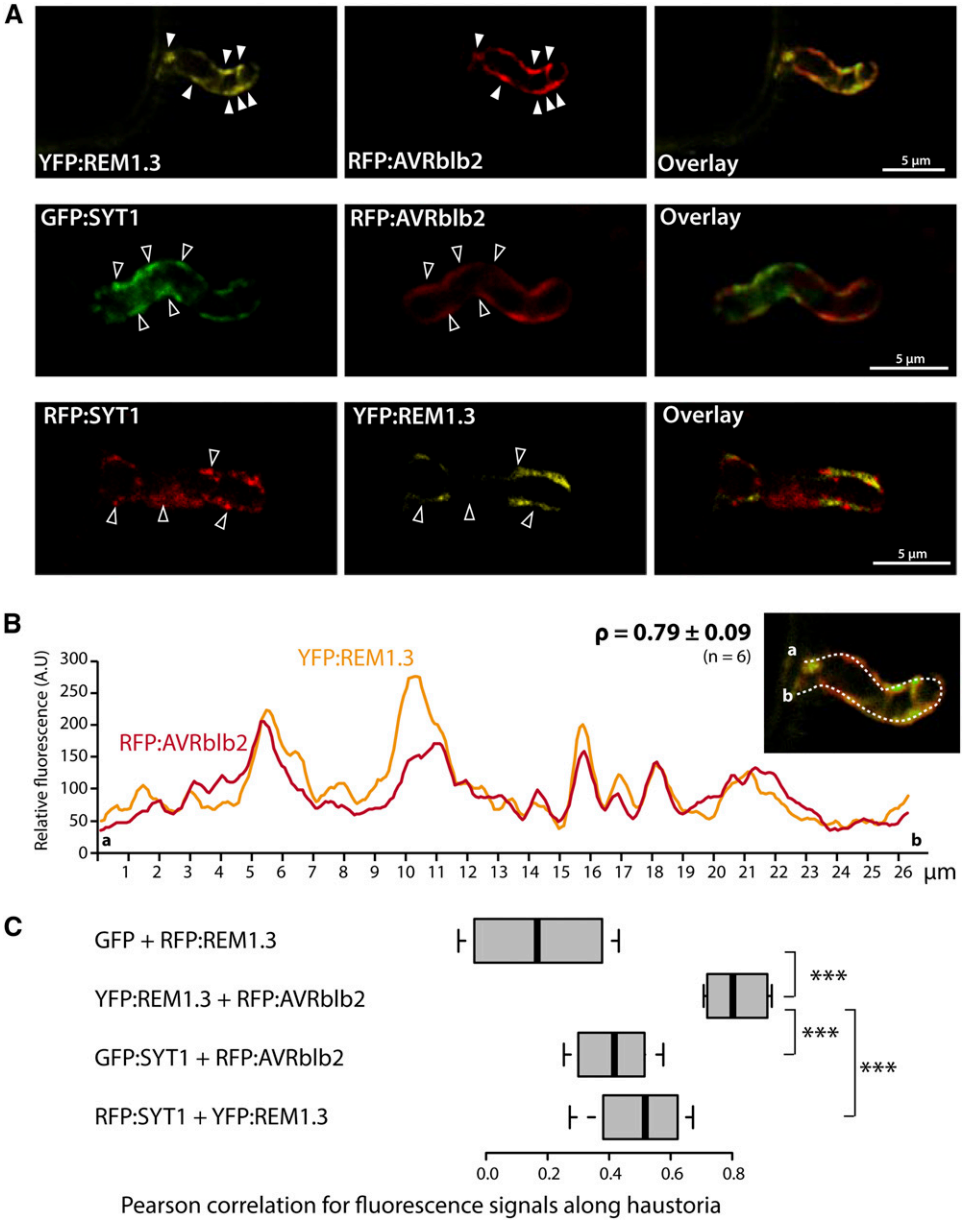

Figure 3. REM1.3 colocalizes with the *P. infestans* RXLR effector AVRblb2 in domains around haustoria. A, Coexpression of EHM markers by *A. tumefaciens*-mediated transient transformation under the control of the CaMV *35S* promoter in haustoriated cells reveals perihaustorial membrane domains. Left, YFP:REM1.3 and RFP:AVRblb2 show nearly full colocalization around haustoria, with all domains strongly labeled by YFP:REM1.3 (closed arrowheads) showing intense RFP fluorescence. Middle, SYT1 strongly labels domains that are only weakly labeled by RFP:AVRblb2 (open arrowheads). Right, SYT1 labels domains around haustoria that are not or weakly labeled by YFP:REM1.3 (open arrowheads). B, Correlation between the RFP and YFP fluorescence signals around haustoria in cells coexpressing RFP:AVRblb2 and YFP:REM1.3. The fluorescence is measured along the dotted line connecting points a and b, as shown in the inset. The average Pearson correlation coefficient for RFP and YFP fluorescence signals along six different perihaustorial membranes is 0.79. A.U., Arbitrary units. C, Quantification of fluorescence correlation for perihaustorial markers highlights the existence of at least two types of domains around haustoria. Pearson correlation coefficients were calculated in cells coexpressing free GFP+RFP:REM1.3, YFP:REM1.3+RFP:AVRblb2, GFP:SYT1+RFP:AVRblb2, and GFP:SYT1+RFP:REM1.3. Only cells in which REM1.3 accumulated around haustoria were considered. Significant differences of the means were assessed using Welch's *t* test (***$P <$ 0.001). Measurements were performed over at least two independent inoculation events.

SYT1, another plant PM-associated protein localized around haustoria (Lu et al., 2012). SYT1 localized in foci around haustoria mostly distinct from foci labeled by AVRblb2 and REM1.3 (Fig. 3A). Since our aim was to characterize perihaustorial domains, we focused the next steps of the analysis on haustoriated cells in which REM1.3 accumulated around haustoria. First, to estimate the background correlation associated with the bleed through of fluorescence, we calculated ρ for the fluorescence signals along haustoria in cells expressing free GFP and RFP:REM1.3. We obtained an average ρ of approximately 0.1, indicating that the GFP and REM1.3 do not colocalize along haustoria (Fig. 3C). Second, we calculated ρ for cells expressing YFP:REM1.3 and RFP:AVRblb2 and obtained an average ρ of approximately 0.8. Third, we calculated ρ for cells expressing GFP:SYT1 and RFP:AVRblb2 as well as RFP:SYT1+YFP:REM1.3. We obtained average ρ values of approximately 0.4 and 0.5, respectively. To test whether colocalization between YFP:REM1.3 and AVRblb2:RFP was significantly higher than between free GFP and RFP:REM1.3, GFP:SYT1 and RFP:AVRblb2, or RFP:SYT1 and YFP:REM1.3, we used Welch's t test. We obtained $P < 0.001$, indicating that correlation between YFP:REM1.3 and AVRblb2:RFP can be considered higher than the others with 99.9% confidence.

Superresolution Structured Illumination Microscopy Confirms the Occurrence of REM1.3 Microdomains at the EHM

To discriminate subcellular compartments accumulating around haustoria and validate the observation of different domains at the EHM with a resolution of approximately 100 nm, we conducted similar experiments using superresolution imaging by structured illumination microscopy (SIM) in *N. benthamiana* (Gutierrez et al., 2010). These experiments again revealed EHM subdomains colabeled by REM1.3 and AVRblb2 but differentially labeled by SYT1 (Fig. 4; Supplemental Movies S1–S3). Altogether, these results demonstrate the high-resolution colocalization of REM1.3 and AVRblb2, supporting their localization to the EHM and the lateral compartmentalization of the EHM into multiple domains.

REM1.3 Overexpression Increases Susceptibility to *P. infestans* in *N. benthamiana*

The recruitment of REM1.3 to domains around active haustoria prompted us to test whether REM1.3 plays a role in susceptibility to *P. infestans*. For this, we analyzed the phenotype of transgenic plants

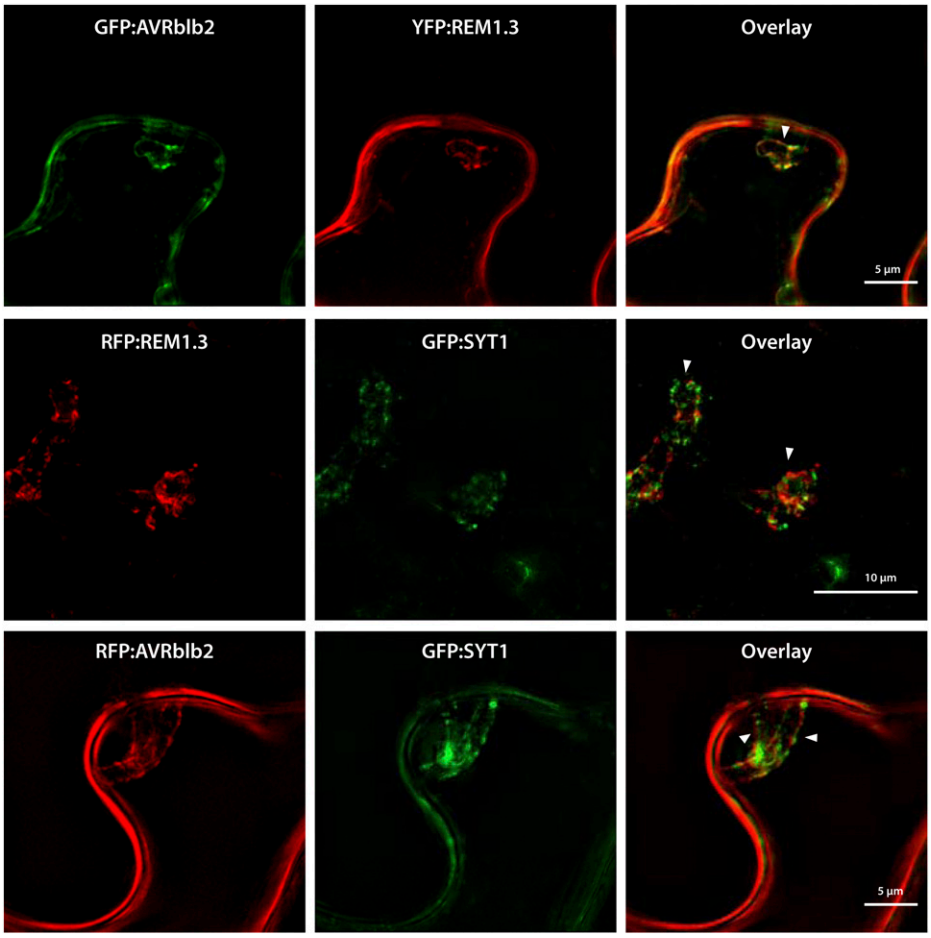

Figure 4. Validation of the occurrence of subdomains at the EHM using superresolution microscopy. YFP:REM1.3 and RFP:AVRblb2 show perfect localization at the EHM mainly at some foci (top row), while GFP:SYT1 labels different microdomains compared with RFP:REM1.3 (middle row). Consistently, RFP:AVRblb2 and GFP:SYT1 also label different domains across the EHM (bottom row). Recombinant constructs were delivered using *A. tumefaciens*-mediated transformation. Images were obtained at 3 dpi using superresolution SIM. Images shown are maximal projections of 31, 30, and 27 frames with 0.11, 0.11, and 0.12 μm steps for the top, middle, and bottom rows, respectively.

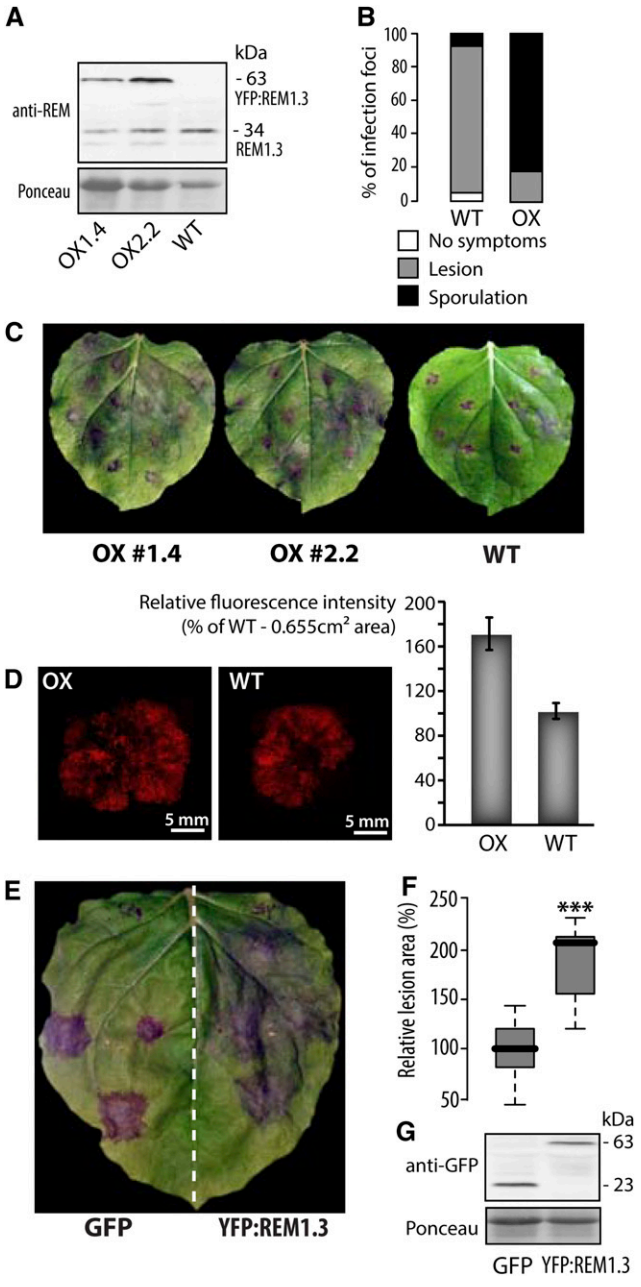

Figure 5. REM1.3 overexpression increases susceptibility to *P. infestans* in *N. benthamiana*. A, Validation of YFP:REM1.3 overexpression in *N. benthamiana* transgenic plants by anti-remorin western blot in two independent *35S*-YFP:REM1.3 lines (OX1.4 and OX2.2) compared with wild-type plants (WT). B, Type and frequency of symptoms caused by *P. infestans* 88069 at 5 dpi on overexpression and wild-type plants as a percentage of 40 infection foci over three independent experiments including three independent overexpression lines. C, Representative images of symptoms caused by *P. infestans* 88069 on *N. benthamiana* overexpression and wild-type plants at 5 dpi. D, Quantification of *P. infestans* 88069td growth in *N. benthamiana* lines by measurement of RFP fluorescence. Representative fluorescence images show *P. infestans* 88069td growth in overexpression and wild-type plants at 4 dpi. Bars = 5 mm. Histograms show relative fluorescence intensity, calculated as the mean pixel intensity over a 0.655-cm^2 image centered on the lesion and expressed as a percentage of the intensity measured on wild-type plants. Three to six images were analyzed per *N. benthamiana* line, and error bars show SD. E, *N. benthamiana* leaf infiltrated with *A. tumefaciens* carrying either *35S*-GFP or *35S*-YFP:REM1.3 (left and right, respectively) and inoculated with *P. infestans* 88069 24 h later. Images were taken and the size of lesions measured at 5 dpi. F, Relative *P. infestans* lesion size on half-leaves infiltrated with *35S*-GFP and *35S*-YFP:REM1.3. Significance was assayed using Student's *t* test (***$P < 0.01$) over 12 lesions in three independent experiments. G, Total proteins extracted from half-leaves infiltrated with *35S*-GFP and *35S*-YFP:REM1.3 and probed by anti-GFP western blots showing similar expression levels for GFP and YFP:REM1.3 constructs.

constitutively expressing YFP:REM1.3 (overexpression). We first verified the expression and integrity of the YFP:REM1.3 fusion protein in these plants using anti-remorin western-blot analysis (Fig. 5A). We next tested the response of these plants to *P. infestans* using zoospore solution droplet inoculation. We counted the proportion of inoculated sites showing no symptoms, necrotic lesions, or *P. infestans* sporulation in control (wild-type) and overexpression plants. We found that the frequency of *P. infestans* sporulation correlated with higher REM1.3 accumulation, whereas the frequency of inoculated areas with no symptom correlated with reduced REM1.3 accumulation (Fig. 5B). At 5 dpi, lesions caused by *P. infestans* growth almost completely covered overexpression plant leaves, whereas the lesions extended slightly beyond the zoospore droplets in wild-type plants at this stage (Fig. 5C). Using image analysis to quantify the surface occupied by hyphae of *P. infestans* 88069td, we found an approximately 1.5-fold increase in overexpression plants compared with controls (Fig. 5D). We also used transient *A. tumefaciens*-mediated overexpression of YFP:REM1.3 in *N. benthamiana*. In half-leaves overexpressing REM1.3, the infected area was on average twice as large as in half-leaves overexpressing GFP (Fig. 5, E and F), indicating that REM1.3 overexpression enhanced susceptibility to *P. infestans*. Quantification of the fluorescence due to GFP and YFP expression as well as anti-GFP western-blot analysis performed on total protein extracts allowed us to select for leaves in which the two *A. tumefaciens*-delivered constructs were expressed to similar levels (Fig. 5G). Taken together, these results indicate a positive role for REM1.3 in susceptibility toward *P. infestans*.

Silencing of REM1.3 Enhances Resistance to *P. infestans* in *N. benthamiana*

To further validate the role of REM1.3 in response to *P. infestans*, we first conducted a phylogenetic analysis to identify REM1.3 orthologs in *N. benthamiana*. We found three REM1.3 orthologs in the *N. benthamiana* genome (Supplemental Fig. S1; Supplemental Data S1). Then, we used a virus-induced gene silencing (VIGS) approach to silence the REM1.3 orthologs in *N. benthamiana* using the tobacco rattle virus pTV00 vector (Ratcliff et al., 2001; Supplemental Fig. S1). Eighteen

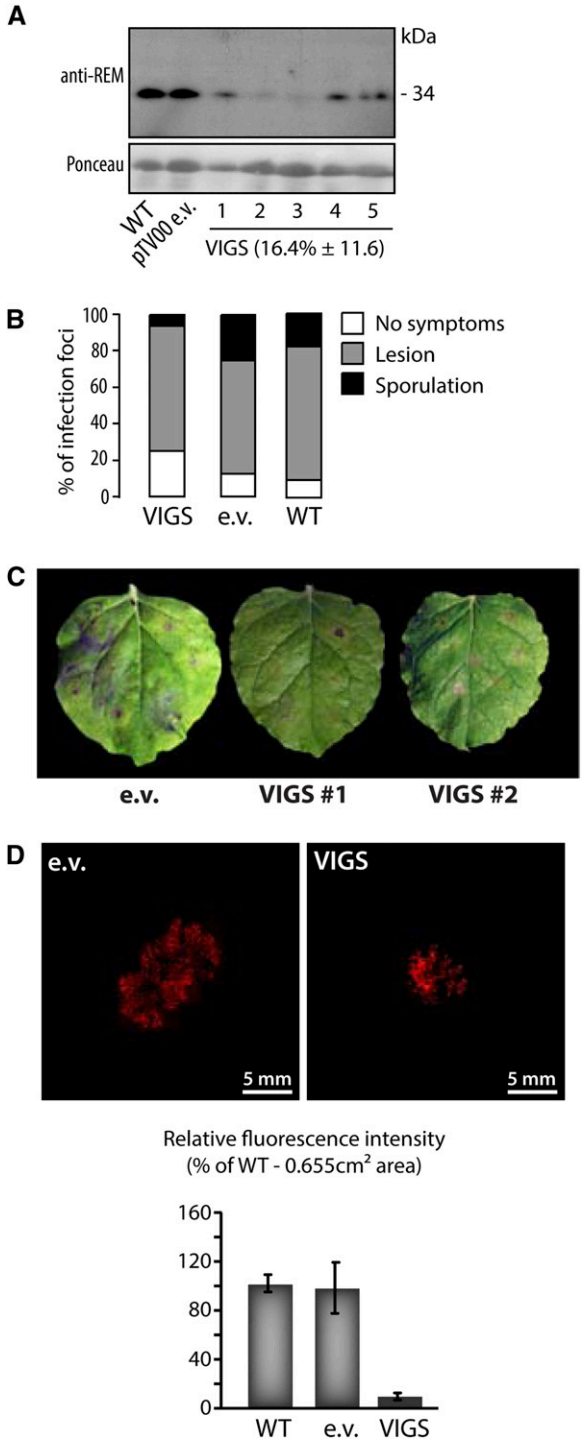

Figure 6. Silencing of REM1.3 enhances resistance to *P. infestans* in *N. benthamiana*. A, Validation of the silencing of REM1.3 orthologs in *N. benthamiana* by anti-REM western blot. The REM1.3 protein amount was estimated based on the western-blot signal. B, Type and frequency of symptoms caused by *P. infestans* 88069 at 6 dpi as a percentage of at least 12 infection foci over three independent experiments. C, Representative images of symptoms caused by *P. infestans* 88069 on *N. benthamiana* at 7 dpi. D, Top, representative fluorescence images showing *P. infestans* 88069td growth at 4 dpi. Bars = 5 mm. Bottom, quantification of *P. infestans* 88069td growth in *N. benthamiana* lines by measurement of RFP fluorescence. Histograms show relative fluorescence intensity calculated as for Figure 5. Three to six images were analyzed per *N. benthamiana* line, and error bars show SD. e.v., Plants infiltrated with the pTV00 empty vector; VIGS, plants infiltrated with the REM1.3 VIGS silencing construct; WT, wild-type plants.

days after delivery of the remorin-silencing construct, but not with the empty vector control (pTV00), we observed a strong decrease in YFP fluorescence in *N. benthamiana* plants stably expressing YFP:REM1.3, validating the efficiency of silencing (Supplemental Fig. S2). In addition, anti-remorin western-blot analysis of total protein extracts from wild-type and silenced (VIGS) *N. benthamiana* plants confirmed the suppression of REM1.3 accumulation by our silencing construct (Fig. 6A). Six-week-old silenced plants did not show any apparent developmental phenotype (Supplemental Fig. S2). We then tested the response of silenced plants to *P. infestans* using zoospore solution droplet inoculation. At 5 dpi, approximately 20% of infection foci in virus-free (wild-type) plants and control plants expressing the pTV00 empty vector showed sporulation, whereas this proportion was less than 5% for foci in silenced plants (Fig. 6B). Conversely, although 20% of infection foci in silenced plants did not show any symptoms, this proportion was reduced to less than 10% in virus-free and empty vector control plants. At 7 dpi, confluent lesions caused by *P. infestans* growth were clearly visible on control plants, whereas the lesions hardly extended beyond the zoospore droplets in silenced plants (Fig. 6C). To confirm that lesion size correlates with pathogen growth in these plants, we used image analysis to quantify the surface occupied by hyphae of *P. infestans* 88069td. We measured an approximately 10-fold decrease in the surface colonized by *P. infestans* 88069td in silenced plants compared with control plants (Fig. 6D).

REM1.3 Promotes Susceptibility to *P. infestans* in Tomato

Most cultivated plants in the Solanaceae family, including tomato and potato, are susceptible to *P. infestans*. To test whether the function of remorin in the *N. benthamiana* response to *P. infestans* is conserved in economically important crops, we inoculated zoospores of *P. infestans* on tomato transgenic plants expressing sense and antisense constructs for the REM1.3 tomato ortholog (Raffaele et al., 2009). The level of REM1.3 in individual plants relative to the wild type was evaluated by anti-remorin western-blot analysis prior to infection (Supplemental Fig. S3). In plants overexpressing REM1.3, *P. infestans*-induced lesions appeared significantly larger than in wild-type and control plants (150% of the wild type on average and up to 300%; Fig. 7). Conversely, plants expressing an antisense REM1.3 construct showed reduced lesions (75% of the wild type on average). Statistics calculated on approximately 50 infection foci per line supported the conclusion that REM1.3 promotes susceptibility to *P. infestans* in tomato. We observed a similar degree of

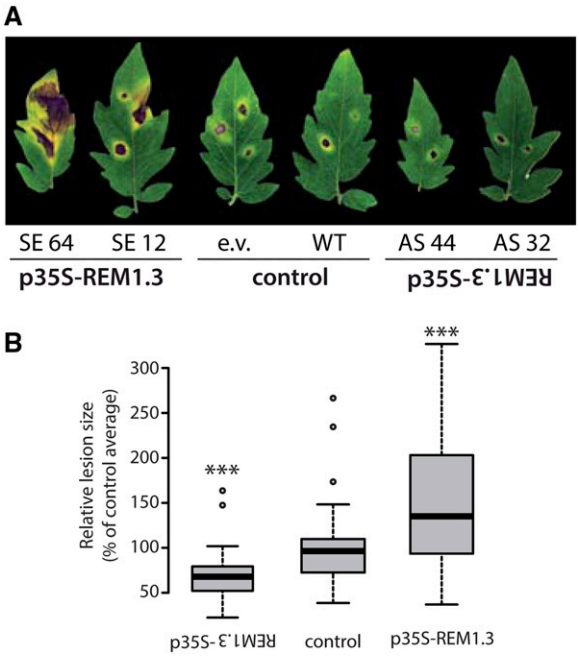

Figure 7. The REM1.3 ortholog promotes susceptibility to *P. infestans* in tomato. A, Symptoms caused by *P. infestans* 88069 at 4 dpi on tomato plants overexpressing a tomato REM1.3 ortholog (SE), empty vector-transformed plants (e.v.), and wild-type (WT) and REM1.3 antisense (AS) plants. B, Box plot showing the distribution of the relative sizes of lesions at 4 dpi on tomato plants with different levels of REM1.3. At least 48 infection foci were measured per line over three independent experiments. The significance of differences compared with the wild type was assessed by Student's *t* test (***$P < 0.01$). Overexpression and silencing of REM were verified by western-blot analysis of individual plants (Supplemental Fig. S3).

increase in *P. infestans* infection in *N. benthamiana* plants overexpressing YFP:REM1.3 and in tomato plants overexpressing untagged REM1.3, indicating that these REM1.3 orthologs have similar functions in response to *P. infestans*, the YFP tag does not significantly alter this function, and the molecular mechanisms underlying this function are conserved in *N. benthamiana* and tomato.

The REM1.3 Membrane Anchor Is Required for Relocalization at the EHM

We recently demonstrated that REM1.3 is targeted to the PM through direct lipid binding of a C-terminal α-helical domain named RemCA (Perraki et al., 2012). To test whether REM1.3 PM binding is also required for relocalization around haustoria, we expressed YFP-tagged wild-type and mutant REM1.3 constructs in *N. benthamiana* using *A. tumefaciens*-mediated transformation. Consistent with previous reports, YFP:REM1.3 localized exclusively at the PM, whereas mutants lacking the RemCA domain (YFP:REM1.3ΔCA) or mutated in the RemCA domain (YFP:REM1.3*) localized to the cytoplasm in noninfected *N. benthamiana* epidermal cells (Fig. 8A). We subsequently inoculated transformed leaves with *P. infestans* 88069td and observed haustoria formed in transformed cells at 4 and 5 dpi. As reported earlier, a strong YFP accumulation is visible around approximately 50% of haustoria formed in YFP:REM1.3-expressing cells. By contrast, a uniform cytoplasmic YFP localization is seen in YFP:REM1.3ΔCA- and YFP:REM1.3*-expressing cells, and none of the haustoria observed in these cells showed any accumulation of YFP fluorescence (more than 30 haustoria surveyed for each construct; Fig. 8B). Therefore, the RemCA membrane anchor is required for REM1.3 relocalization around *P. infestans* haustoria.

The REM1.3 Membrane Anchor Is Required for the Promotion of Susceptibility to *P. infestans*

To test whether the REM1.3 membrane-binding domain is required for the promotion of susceptibility to *P. infestans*, we measured *P. infestans* lesion size

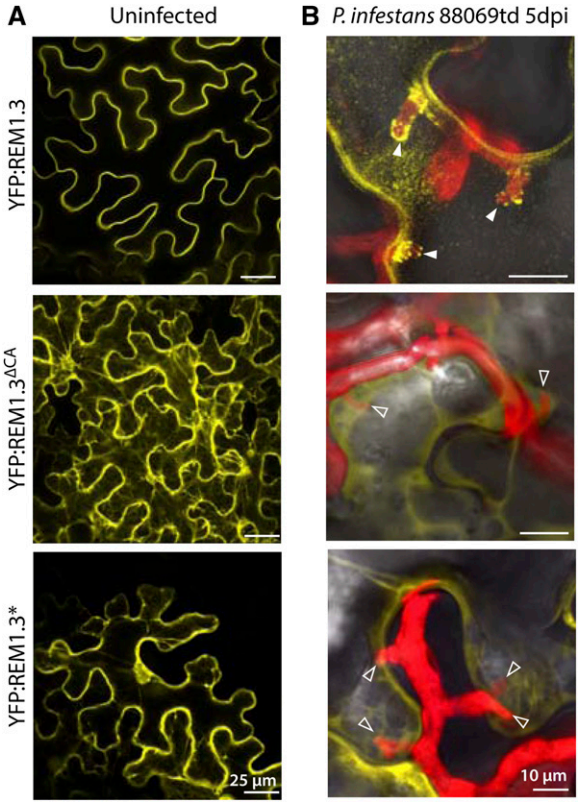

Figure 8. The REM1.3 membrane-binding domain is required for perihaustorial targeting. Confocal micrographs show the subcellular localization of YFP fusions with wild-type REM1.3, REM1.3 lacking the C-terminal membrane anchor domain (ΔCA), and REM1.3 with mutated C-terminal membrane anchor domain (*) in uninfected cells (A) and cells infected by *P. infestans* 88069td (B). The tips of haustoria are shown by closed arrowheads when surrounded by YFP labeling and with open arrowheads otherwise. Constructs controlled by the *35S* promoter were delivered using *A. tumefaciens*-mediated transformation. Images shown are single optical plane sections except for uninfected cells expressing YFP:REM1.3$^{\Delta CA}$ and YFP:REM1.3*, which correspond to maximal projections of 32 frames with 1 μm steps.

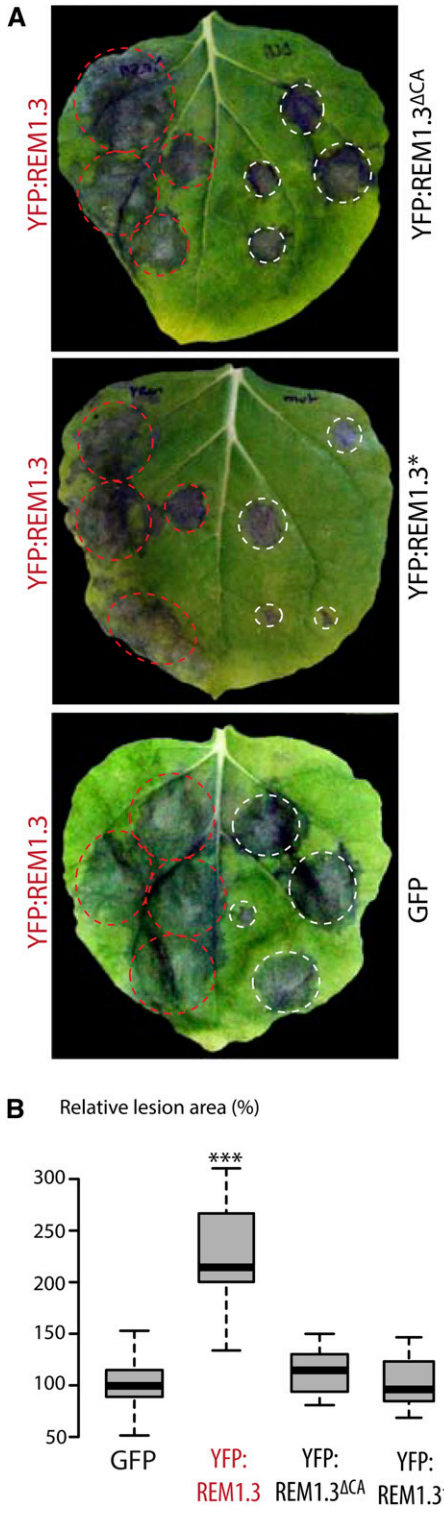

Figure 9. The REM1.3 membrane anchor is required for the promotion of susceptibility to *P. infestans*. A, Symptoms caused by *P. infestans* 88069 at 5 dpi on leaves transiently overexpressing YFP fusions with wild-type REM1.3 on one half and free GFP or REM1.3 lacking the C-terminal membrane anchor domain (ΔCA) or REM1.3 with mutated C-terminal membrane anchor domain (*) on the other half. B, Box plot showing relative sizes of the lesions over 12 to 54 infection foci in three independent experiments. Significance of differences compared with GFP-expressing leaves was assessed by Student's *t* test (***$P < 0.01$). Constructs controlled by the *35S* promoter were delivered using *A. tumefaciens*-mediated transformation; their expression was verified by detection of fluorescence.

formed on *N. benthamiana* leaves expressing full-length or mutated REM1.3 constructs. Half-leaves expressing YFP:REM1.3 showed lesions approximately 250% the size of half-leaves expressing the GFP control, whereas sectors expressing YFP:REM1.3ΔCA or YFP:REM1.3* showed lesions the same size as on half-leaves infiltrated with the GFP control (Fig. 9). These results indicate that the RemCA membrane anchor is required for REM1.3 function in susceptibility to *P. infestans*. This also suggests that REM1.3 localization to microdomains, either at the PM or at the EHM, is essential for the promotion of susceptibility to *P. infestans*.

DISCUSSION

The EHM is a critical interface between eukaryotic pathogens and plants, yet we know little about its biogenesis, composition, and function. To gain insights into the biology of the EHM, we investigated the role of REM1.3, one of two plant membrane proteins known to accumulate around haustoria during infection of *N. benthamiana* by *P. infestans* (Lu et al., 2012). We used a combination of cell biology and pathology assays to demonstrate the localization of REM1.3 into discrete perihaustorial domains that are also labeled by the *P. infestans* RXLR effector AVRblb2. Genetic analyses revealed that REM1.3 enhances *P. infestans* colonization and, therefore, can be considered a susceptibility factor (Van Damme et al., 2005; Pavan et al., 2010). Thus, to our knowledge, REM1.3 is the first plant susceptibility protein to localize at the haustorial interface, supporting the view that plant pathogens are likely to perturb host membrane processes to promote intracellular accommodation inside host cells and infection.

Although many plant PM proteins are excluded from the EHM, REM1.3 appears to localize to discrete domains around haustoria, presumably at the EHM. Such REM1.3 domains could also reside in the extrahaustorial matrix between the EHM and the oomycete haustorial cell wall, although this is less likely, since REM1.3 was shown to localize to the cytoplasmic leaflet of the plant PM (Raffaele et al., 2009). Indeed, REM1.3 is a well-established plant membrane raft marker protein that binds directly to negatively charged lipids that are enriched in plant membrane rafts (Raffaele et al., 2009; Furt et al., 2010; Perraki et al., 2012). The association of REM1.3 with the EHM suggests that this membrane may have a lipid composition close to that of membrane rafts. Similarly, the peribacteroid membrane that is formed during bacterial endosymbiosis in plants also shares similarities

with membrane rafts (Pumplin and Harrison, 2009; Lefebvre et al., 2010). Bhat et al. (2005) reported that plant membrane proteins such as the barley (*Hordeum vulgare*) MILDEW RESISTANCE PROTEIN O, the barley syntaxin REQUIRED FOR MLO-SPECIFIED RESISTANCE2 (ROR2), and the Arabidopsis syntaxin PENETRATION1 (PEN1) redistribute toward *Blumeria graminis* f. sp. *hordei* penetration sites during infection. These penetration sites are strongly stained by the filipin dye, indicating abundance in sterols and leading the authors to propose that membrane raft-like domains form below the appressoria of mildew fungi (Bhat et al., 2005; Bhat and Panstruga, 2005).

Accumulating evidence suggests that pathogens manipulate host cells to establish perimicrobial domains with a specific lipid composition (Cossart and Roy, 2010; Ham et al., 2011; Gu and Innes, 2012). What could be the functional and evolutionary advantages of establishing sterol- and sphingolipid-rich perihaustorial membrane compartments? The altered lipid composition of the EHM may enable directional transfer of molecules, nutrients, and effectors through the pathogen membrane and the host-derived membrane. In addition, sterols and sphingolipids, the major lipid components of membrane rafts, are very diverse lipid groups, including several plant-specific forms (Suzuki and Muranaka, 2007; Pata et al., 2010; Cacas et al., 2012). These lipids, therefore, may constitute a signature of the host membrane that haustoria-forming pathogens evolved to target and manipulate.

The perihaustorial membrane domains containing REM1.3 colocalize with the *P. infestans* host-translocated effector AVRblb2, one of a handful RXLR-type effectors known to localize around haustoria in infected plant cells (Bozkurt et al., 2011, 2012; Saunders et al., 2012). Functional analyses indicated that host membrane targeting is crucial for the promotion of susceptibility by AVRblb2 (Bozkurt et al., 2011). AVRblb2 prevents the secretion of the C14 defense protease, possibly during the release or fusion of secretory vesicles to the EHM (Bozkurt et al., 2011). These findings point toward a critical role for the control of plant vesicle trafficking for the establishment of virulence, as shown in animal-microbe interactions (Baxt et al., 2013). In addition, oomycete effectors could possibly trigger host membrane reorganization into coalesced membrane rafts, with a similar mechanism reported for some proteinaceous toxins (García-Sáez et al., 2011). Proteins in the remorin family were proposed to control PM lateral organization (Jarsch and Ott, 2011). Their accumulation in particular membrane domains may facilitate the action of membrane-targeted effectors or drive the segregation of effectors into specific membrane domains. Our finding that the AVRblb2 effector colocalizes with the host susceptibility protein REM1.3 supports the hypothesis that filamentous plant pathogen effectors exploit host membrane lateral organization to accommodate infection structures (Bhat et al., 2005; Caillaud et al., 2012).

Using overexpression of fusion proteins, we observed that REM1.3 showed perihaustorial distribution in only about half the cases, whereas AVRblb2 always localized around haustoria. Whether the frequency of accumulation around haustoria is influenced by the delivery method remains to be determined. Differential protein accumulation around haustoria may also be due to dynamic temporal events during haustorial biogenesis. One possibility is that effectors secreted from haustoria could mediate the recruitment of REM1.3 from the EHM or that REM1.3 slowly accumulates in time to reach detectable levels at the EHM. Therefore, the accumulation of REM1.3 around haustoria may result from selective trafficking toward haustoria or from specific binding to lipids enriched around haustoria (Perraki et al., 2012).

Differential labeling of REM1.3 and AVRblb2 versus SYT1 at the EHM shows that, rather than being uniform, the EHM is a patchwork formed by multiple subdomains. What are the implications of the occurrence of multiple microdomains at the EHM? The functions of these domains remain unclear. It is possible that these are sites where diverse haustorial activities, such as endocytosis or exocytosis, are regulated to achieve efficient macromolecule exchange. Future studies will reveal which endomembrane pathways contribute to the formation of the EHM microdomains and uncover the roles that these trafficking pathways play in plant immunity.

MATERIALS AND METHODS

Plant Lines and Growth Conditions

Leaves from 5-week-old *Nicotiana benthamiana* and tomato (*Solanum lycopersicum* 'Ailsa Craig') plants grown in a growth chamber at 25°C under 16-h-day/8-h-night conditions were used for all experiments. *35S*-YFP:REM1.3 transgenic *N. benthamiana* plants expressing the potato (*Solanum tuberosum*) REM1.3 ortholog (StREM1.3) were obtained from Lu et al. (2012), and T2 plants were screened using YFP fluorescence observed with a confocal microscope. Sense and antisense tomato plants misexpressing the tomato REM1.3 ortholog (SlREM1.2) were obtained from Raffaele et al. (2009). All tomato plants used were T3 and T4 plants and were screened by protein gel-blot analysis using anti-remorin (Raffaele et al., 2009) antibodies. Protein-blot signal was quantified using the gel analysis function in ImageJ, and only plants belonging to the bottom and top quartiles for REM1.3 level were considered as antisense and sense plants, respectively (corresponding to remorin at less than approximately 80% and more than approximately 150% of the wild-type level, respectively; Supplemental Fig. S3).

Cloning Procedures and Plasmid Constructs

The *35S*-YFP:StREM1.3 construct was obtained from Raffaele et al. (2009), the *35S*-RFP:AVRblb2 construct from Bozkurt et al. (2011), the *35S*-YFP:StREM1.3* and *35S*-YFP:StREM1.3ΔCA constructs from Perraki et al. (2012), and the GFP:HaRXL17 construct from Caillaud et al. (2012). The *35S*-RFP:StREM1.3 construct was generated using classical Gateway cloning into the pH7WGR2 vector (Karimi et al., 2002). The *35S*-GFP:SYT1 and *35S*-RFP:SYT1 constructs were generated from specific amplification of *N. benthamiana* complementary DNAs with the 5′-AAAAAGCAGGCTTCATGGGTTTTGTGAGTACTATA-3′ and 5′-AGAAAGCTGGGTCTCATGATGCAGTTCTCCATTG-3′ primers and classical Gateway cloning into the pk7WGF2 and pH7WGR2 vectors. To design the remorin-silencing construct, we first performed a phylogenetic analysis on Remorin_C domains using remorin sequences identified in the *N. benthamiana* genome version 0.4.4, the tomato

genome International Tomato Annotation Group release 2.3, the potato genome Potato Genome Sequencing Consortium DM 3.4, and the Arabidopsis (*Arabidopsis thaliana*) genome (Supplemental Fig. S1A). A 101-amino acid alignment of a conserved region was constructed using MUSCLE and used as input in Phylip (Felsenstein, 1989) to build a consensus parsimony tree after a 100-replicate bootstrap analysis. This analysis revealed three orthologs of REM1.3 in *N. benthamiana* (Supplemental Fig. S1A). We selected a silencing construct covering 178 nucleotides at the C terminus of the REM1.3 sequence. Using homemade perl scripts, we predicted this construct to generate 16 putative 21-nucleotide small interfering RNA species, with three putative targets in the *N. benthamiana* genome, corresponding to the three REM1.3 orthologs (Supplemental Fig. S1B). The VIGS construct was generated by PCR amplification using full-length StREM1.3 as a template with forward primers including a *Bam*HI restriction site and reverse primers including a *Kpn*I restriction site. PCR products were digested with *Bam*HI and *Kpn*I and ligated into the *Agrobacterium tumefaciens* binary tobacco rattle virus vector pTV00 (Ratcliff et al., 2001). Silencing experiments were performed as described (Bos et al., 2010) using pTV00 empty vector as a negative control and pTV00 carrying the *N. benthamiana* phytoene desaturase gene fragment as a silencing control. Remorin silencing was verified by loss of fluorescence in *35S*-YFP:REM1.3 stable transgenic plants and anti-remorin western-blot analysis.

Transient Expression in Planta

A. tumefaciens GV3101 was used to deliver transfer DNA constructs into 3-week-old *N. benthamiana* plants. Overnight, *A. tumefaciens* cultures were harvested by centrifugation at 10,000*g*, resuspended in infiltration medium (10 mM $MgCl_2$, 5 mM MES, pH 5.3, and 150 mM acetosyringone) prior to syringe infiltration into either the entire leaf or leaf sections. For confocal microscopy, constructs were infiltrated to a final optical density at 600 nm (OD_{600}) = 0.4, in equal amounts in the case of coinfiltrations. For transient protein expression followed by *Phytophthora infestans* inoculation, the constructs were infiltrated to OD_{600} = 0.3 supplemented with p19 silencing suppressor to OD_{600} = 0.1, and *P. infestans* was inoculated 24 h later. For VIGS silencing, pTV00 and pBINTRA constructs were coinfiltrated at OD_{600} = 0.3 and OD_{600} = 0.2, respectively.

Confocal Microscopy

Imaging was performed on a Leica TCS SP5 confocal microscope (Leica Microsystems) using 20×, 40× air, and 63× water-immersion objectives. REM1.3 localization studies were performed with tagged StREM1.3 constructs. Excitation wavelengths and filters for emission spectra were set as described (Lu et al., 2012). Colocalization images were taken using sequential scanning between lines. Image analysis was done with the Leica LAS AF software, ImageJ (1.43u), and Adobe Photoshop CS4 (11.0). Callose staining and imaging were performed as described (Bozkurt et al., 2011). The superresolution images were taken on a Zeiss Elyra PS1 structured illumination microscope using a 63× water objective. The GFP and RFP probes were excited using 488- and 561-nm laser diodes, and their fluorescence emission was collected at 495 to 550 nm and 570 to 620 nm, respectively. To generate a single three-dimensional SIM image, 15 raw images were collected (five phases and three rotations), and the data were processed using Zeiss Zen Black software. GFP and RFP were collected sequentially, and the SIM images were color aligned using the channel alignment tool in Zen (calibration beads were taken at the end of an experiment and used to generate an alignment matrix).

Pathogenicity Assays

Unless stated otherwise, *P. infestans* infection assays were performed by inoculation with 10-μL droplets of zoospore solution at 50 zoospores per microliter on detached *N. benthamiana* leaves (Chaparro-Garcia et al., 2011). *P. infestans* isolate 88069 (van West et al., 1999) and a transformant expressing a cytosolic tandem DsRed protein (88069td; Whisson et al., 2007) were used. For transient protein expression followed by *P. infestans* inoculation, half of the leaf was infiltrated with *A. tumefaciens* carrying the *35S*-GFP construct as a control and the other half with a strain carrying the *35S*-YFP:StREM1.3 construct. Constructs were expressed by *A. tumefaciens*-mediated transformation together with p19 silencing suppressor 24 h prior to *P. infestans* inoculation. Lesion sizes were calculated on images taken at 5 dpi, analyzed using area measurements in ImageJ (1.43u).

Protein Extraction and Immunoblots

Proteins were transiently expressed by *A. tumefaciens* in *N. benthamiana* leaves and harvested 2 d post infiltration. Protein extracts were prepared by grinding leaf samples in liquid nitrogen and extracting 1 g of tissue in 3 mL of GTEN protein extraction buffer (150 mM Tris-HCl, pH 7.5, 150 mM NaCl, 10% (w/v) glycerol, and 10 mM EDTA) and freshly added 10 mM dithiothreitol, 2% (w/v) polyvinylpolypyrrolidone, 1% (v/v) protease inhibitor cocktail (Sigma), and 1% (v/v) Nonidet P-40 according to Win et al. (2011). Anti-remorin (Raffaele et al., 2009) and commercial anti-GFP (Invitrogen) were used as primary antibodies. Western-blot signal was quantified using gel analysis in ImageJ (1.43u) and normalized based on the quantification of total proteins stained by Ponceau Red.

Supplemental Data

The following materials are available in the online version of this article.

Supplemental Figure S1. Phylogeny of *N. benthamiana* remorins and design of a REM1.3 VIGS silencing construct.

Supplemental Figure S2. Characterization of *N. benthamiana* plants silenced for REM1.3.

Supplemental Figure S3. Details of the molecular and phenotypic characterization of tomato transgenic lines misexpressing the tomato REM1.3 ortholog (SlREM1.2).

Supplemental Data S1. Multiple sequence alignment used for the generation of the parsimony tree in Supplemental Figure S1.

Supplemental Movie S1. Three-dimensional imaging of YFP:REM1.3 with RFP:AVRblb2 colocalization at the EHM using superresolution microscopy.

Supplemental Movie S2. Three-dimensional imaging of discrete EHM domains marked by RFP:REM1.3 with GFP:SYT1 at the EHM using superresolution microscopy.

Supplemental Movie S3. Three-dimensional imaging of discrete EHM domains marked by RFP:AVRblb2 with GFP:SYT1 at the EHM using superresolution microscopy.

ACKNOWLEDGMENTS

We thank Joe Win for help with the design of the remorin-silencing construct, Marie-Cecile Caillaud and Jonathan D.G. Jones for useful comments and providing the GFP:HaRXL17 construct, Steve Whisson for 88069td, and Matthew Smoker and Sebastian Schornack for providing *N. benthamiana* REM1.3-overexpressing lines. We thank Sebastian Schornack, Joe Win, Liliana M. Cano, Angela Chaparro-Garcia, Diane G.O. Saunders, Malick Mbengue, and Silke Robatzek for useful discussions and suggestions.

Received January 15, 2014; accepted May 6, 2014; published May 7, 2014.

LITERATURE CITED

Baxt LA, Garza-Mayers AC, Goldberg MB (2013) Bacterial subversion of host innate immune pathways. Science **340:** 697–701

Benschop JJ, Mohammed S, O'Flaherty M, Heck AJ, Slijper M, Menke FL (2007) Quantitative phosphoproteomics of early elicitor signaling in *Arabidopsis*. Mol Cell Proteomics **6:** 1198–1214

Bhat RA, Miklis M, Schmelzer E, Schulze-Lefert P, Panstruga R (2005) Recruitment and interaction dynamics of plant penetration resistance components in a plasma membrane microdomain. Proc Natl Acad Sci USA **102:** 3135–3140

Bhat RA, Panstruga R (2005) Lipid rafts in plants. Planta **223:** 5–19

Bos JI, Armstrong MR, Gilroy EM, Boevink PC, Hein I, Taylor RM, Zhendong T, Engelhardt S, Vetukuri RR, Harrower B, et al (2010) *Phytophthora infestans* effector AVR3a is essential for virulence and manipulates plant immunity by stabilizing host E3 ligase CMPG1. Proc Natl Acad Sci USA **107:** 9909–9914

Bozkurt TO, Schornack S, Banfield MJ, Kamoun S (2012) Oomycetes, effectors, and all that jazz. Curr Opin Plant Biol **15:** 483–492

Bozkurt TO, Schornack S, Win J, Shindo T, Ilyas M, Oliva R, Cano LM, Jones AME, Huitema E, van der Hoorn RAL, et al (2011) *Phytophthora infestans* effector AVRblb2 prevents secretion of a plant immune protease at the haustorial interface. Proc Natl Acad Sci USA **108:** 20832–20837

Cacas JL, Furt F, Le Guédard M, Schmitter JM, Buré C, Gerbeau-Pissot P, Moreau P, Bessoule JJ, Simon-Plas F, Mongrand S (2012) Lipids of plant membrane rafts. Prog Lipid Res **51:** 272–299

Caillaud MC, Piquerez SJ, Fabro G, Steinbrenner J, Ishaque N, Beynon J, Jones JD (2012) Subcellular localization of the Hpa RxLR effector repertoire identifies a tonoplast-associated protein HaRxL17 that confers enhanced plant susceptibility. Plant J **69:** 252–265

Catanzariti AM, Dodds PN, Lawrence GJ, Ayliffe MA, Ellis JG (2006) Haustorially expressed secreted proteins from flax rust are highly enriched for avirulence elicitors. Plant Cell **18:** 243–256

Chaparro-Garcia A, Wilkinson RC, Gimenez-Ibanez S, Findlay K, Coffey MD, Zipfel C, Rathjen JP, Kamoun S, Schornack S (2011) The receptor-like kinase SERK3/BAK1 is required for basal resistance against the late blight pathogen *Phytophthora infestans* in *Nicotiana benthamiana*. PLoS ONE **6:** e16608

Coffey M, Wilson U (1983) Histology and Cytology of Infection and Disease Caused by Phytophthora. American Phytopathological Society, St. Paul

Cossart P, Roy CR (2010) Manipulation of host membrane machinery by bacterial pathogens. Curr Opin Cell Biol **22:** 547–554

Felsenstein J (1989) PHYLIP: Phylogeny Inference Package (version 3.2). Cladistics **5:** 164–166

Furt F, König S, Bessoule JJ, Sargueil F, Zallot R, Stanislas T, Noirot E, Lherminier J, Simon-Plas F, Heilmann I, et al (2010) Polyphosphoinositides are enriched in plant membrane rafts and form microdomains in the plasma membrane. Plant Physiol **152:** 2173–2187

García-Sáez AJ, Buschhorn SB, Keller H, Anderluh G, Simons K, Schwille P (2011) Oligomerization and pore formation by equinatoxin II inhibit endocytosis and lead to plasma membrane reorganization. J Biol Chem **286:** 37768–37777

Gu Y, Innes RW (2012) The KEEP ON GOING protein of *Arabidopsis* regulates intracellular protein trafficking and is degraded during fungal infection. Plant Cell **24:** 4717–4730

Gutierrez R, Grossmann G, Frommer WB, Ehrhardt DW (2010) Opportunities to explore plant membrane organization with super-resolution microscopy. Plant Physiol **154:** 463–466

Ham H, Sreelatha A, Orth K (2011) Manipulation of host membranes by bacterial effectors. Nat Rev Microbiol **9:** 635–646

Jarsch IK, Ott T (2011) Perspectives on remorin proteins, membrane rafts, and their role during plant-microbe interactions. Mol Plant Microbe Interact **24:** 7–12

Karimi M, Inzé D, Depicker A (2002) Gateway vectors for Agrobacterium-mediated plant transformation. Trends Plant Sci **7:** 193–195

Keinath NF, Kierszniowska S, Lorek J, Bourdais G, Kessler SA, Shimosato-Asano H, Grossniklaus U, Schulze WX, Robatzek S, Panstruga R (2010) PAMP (pathogen-associated molecular pattern)-induced changes in plasma membrane compartmentalization reveal novel components of plant immunity. J Biol Chem **285:** 39140–39149

Kemen E, Jones JD (2012) Obligate biotroph parasitism: can we link genomes to lifestyles? Trends Plant Sci **17:** 448–457

Koh S, André A, Edwards H, Ehrhardt D, Somerville S (2005) *Arabidopsis thaliana* subcellular responses to compatible *Erysiphe cichoracearum* infections. Plant J **44:** 516–529

Lefebvre B, Furt F, Hartmann MA, Michaelson LV, Carde JP, Sargueil-Boiron F, Rossignol M, Napier JA, Cullimore J, Bessoule JJ, et al (2007) Characterization of lipid rafts from *Medicago truncatula* root plasma membranes: a proteomic study reveals the presence of a raft-associated redox system. Plant Physiol **144:** 402–418

Lefebvre B, Timmers T, Mbengue M, Moreau S, Hervé C, Tóth K, Bittencourt-Silvestre J, Klaus D, Deslandes L, Godiard L, et al (2010) A remorin protein interacts with symbiotic receptors and regulates bacterial infection. Proc Natl Acad Sci USA **107:** 2343–2348

Liu J, Elmore JM, Fuglsang AT, Palmgren MG, Staskawicz BJ, Coaker G (2009) RIN4 functions with plasma membrane H^+-ATPases to regulate stomatal apertures during pathogen attack. PLoS Biol **7:** e1000139

Lu YJ, Schornack S, Spallek T, Geldner N, Chory J, Schellmann S, Schumacher K, Kamoun S, Robatzek S (2012) Patterns of plant subcellular responses to successful oomycete infections reveal differences in host cell reprogramming and endocytic trafficking. Cell Microbiol **14:** 682–697

Marín M, Thallmair V, Ott T (2012) The intrinsically disordered N-terminal region of AtREM1.3 remorin protein mediates protein-protein interactions. J Biol Chem **287:** 39982–39991

Micali CO, Neumann U, Grunewald D, Panstruga R, O'Connell R (2011) Biogenesis of a specialized plant-fungal interface during host cell internalization of *Golovinomyces orontii* haustoria. Cell Microbiol **13:** 210–226

Mongrand S, Morel J, Laroche J, Claverol S, Carde JP, Hartmann MA, Bonneu M, Simon-Plas F, Lessire R, Bessoule JJ (2004) Lipid rafts in higher plant cells: purification and characterization of Triton X-100-insoluble microdomains from tobacco plasma membrane. J Biol Chem **279:** 36277–36286

Pata MO, Hannun YA, Ng CK (2010) Plant sphingolipids: decoding the enigma of the sphinx. New Phytol **185:** 611–630

Pavan S, Jacobsen E, Visser RG, Bai Y (2010) Loss of susceptibility as a novel breeding strategy for durable and broad-spectrum resistance. Mol Breed **25:** 1–12

Perraki A, Cacas JL, Crowet JM, Lins L, Castroviejo M, German-Retana S, Mongrand S, Raffaele S (2012) Plasma membrane localization of *Solanum tuberosum* remorin from group 1, homolog 3 is mediated by conformational changes in a novel C-terminal anchor and required for the restriction of potato virus X movement. Plant Physiol **160:** 624–637

Pike LJ (2006) Rafts defined: a report on the Keystone Symposium on Lipid Rafts and Cell Function. J Lipid Res **47:** 1597–1598

Pumplin N, Harrison MJ (2009) Live-cell imaging reveals periarbuscular membrane domains and organelle location in *Medicago truncatula* roots during arbuscular mycorrhizal symbiosis. Plant Physiol **151:** 809–819

Raffaele S, Bayer E, Lafarge D, Cluzet S, German Retana S, Boubekeur T, Leborgne-Castel N, Carde JP, Lherminier J, Noirot E, et al (2009) Remorin, a Solanaceae protein resident in membrane rafts and plasmodesmata, impairs potato virus X movement. Plant Cell **21:** 1541–1555

Raffaele S, Mongrand S, Gamas P, Niebel A, Ott T (2007) Genome-wide annotation of remorins, a plant-specific protein family: evolutionary and functional perspectives. Plant Physiol **145:** 593–600

Ratcliff F, Martin-Hernandez AM, Baulcombe DC (2001) Tobacco rattle virus as a vector for analysis of gene function by silencing. Plant J **25:** 237–245

Reymond P, Kunz B, Paul-Pletzer K, Grimm R, Eckerskorn C, Farmer EE (1996) Cloning of a cDNA encoding a plasma membrane-associated, uronide binding phosphoprotein with physical properties similar to viral movement proteins. Plant Cell **8:** 2265–2276

Saunders DG, Breen S, Win J, Schornack S, Hein I, Bozkurt TO, Champouret N, Vleeshouwers VG, Birch PR, Gilroy EM, et al (2012) Host protein BSL1 associates with *Phytophthora infestans* RXLR effector AVR2 and the *Solanum demissum* immune receptor R2 to mediate disease resistance. Plant Cell **24:** 3420–3434

Schornack S, van Damme M, Bozkurt TO, Cano LM, Smoker M, Thines M, Gaulin E, Kamoun S, Huitema E (2010) Ancient class of translocated oomycete effectors targets the host nucleus. Proc Natl Acad Sci USA **107:** 17421–17426

Shahollari B, Peskan-Berghöfer T, Oelmüller R (2004) Receptor kinases with leucine-rich repeats are enriched in Triton X-100 insoluble plasma membrane microdomains from plants. Physiol Plant **122:** 397–403

Simons K, Gerl MJ (2010) Revitalizing membrane rafts: new tools and insights. Nat Rev Mol Cell Biol **11:** 688–699

Stam R, Jupe J, Howden AJM, Morris JA, Boevink PC, Hedley PE, Huitema E (2013) Identification and characterization of CRN effectors in *Phytophthora capsici* shows modularity and functional diversity. PLoS ONE **8:** e59517

Suzuki M, Muranaka T (2007) Molecular genetics of plant sterol backbone synthesis. Lipids **42:** 47–54

Urbanus SL, Ott T (2012) Plasticity of plasma membrane compartmentalization during plant immune responses. Front Plant Sci **3:** 181

Van Damme M, Andel A, Huibers RP, Panstruga R, Weisbeek PJ, Van den Ackerveken G (2005) Identification of *Arabidopsis* loci required for susceptibility to the downy mildew pathogen *Hyaloperonospora parasitica*. Mol Plant Microbe Interact **18:** 583–592

van Damme M, Zeilmaker T, Elberse J, Andel A, de Sain-van der Velden M, van den Ackerveken G (2009) Downy mildew resistance in *Arabidopsis* by mutation of HOMOSERINE KINASE. Plant Cell **21:** 2179–2189

van West P, Kamoun S, van't Klooster JW, Govers F (1999) Internuclear gene silencing in *Phytophthora infestans*. Mol Cell **3:** 339–348

Voegele RT, Struck C, Hahn M, Mendgen K (2001) The role of haustoria in sugar supply during infection of broad bean by the rust fungus *Uromyces fabae*. Proc Natl Acad Sci USA **98:** 8133–8138

Wang W, Wen Y, Berkey R, Xiao S (2009) Specific targeting of the *Arabidopsis* resistance protein RPW8.2 to the interfacial membrane encasing the fungal haustorium renders broad-spectrum resistance to powdery mildew. Plant Cell **21:** 2898–2913

Whisson SC, Boevink PC, Moleleki L, Avrova AO, Morales JG, Gilroy EM, Armstrong MR, Grouffaud S, van West P, Chapman S, et al (2007) A translocation signal for delivery of oomycete effector proteins into host plant cells. Nature **450:** 115–118

Win J, Chaparro-Garcia A, Belhaj K, Saunders DG, Yoshida K, Dong S, Schornack S, Zipfel C, Robatzek S, Hogenhout SA, et al (2012) Effector biology of plant-associated organisms: concepts and perspectives. Cold Spring Harb Symp Quant Biol **77:** 235–247

Win J, Kamoun S, Jones AM (2011) Purification of effector-target protein complexes via transient expression in *Nicotiana benthamiana*. Methods Mol Biol **712:** 181–194